Desalination and Water Treatment
www.deswater.com

doi: 10.5004/dwt.2020.25701

190 (2020) 247–255
June

Novel magnetic FeS_2/Fe_3O_4 composites as adsorbents for chromium(VI) removal from aqueous solution

Guobao Chen*, Yuanhang Lu, Xinming Zhang

School of Metallurgy, Northeastern University, Shenyang 110819, Liaoning, China, Tel. +86 24 83681319; Fax: +86 24 23906316; emails: chengb@smm.neu.edu.cn (G.B. Chen), cgb8922@163.com (Y.H. Lu), smile1985zll@163.com (X.M. Zhang)

Received 22 July 2019; Accepted 14 February 2020

ABSTRACT

In this study, novel magnetite composite FeS_2/Fe_3O_4 was synthesized by a one-pot hydrothermal method. It is applied as an adsorbent for chromium(VI) removal from aqueous solution. The pyrite (FeS_2) and the magnetite (Fe_3O_4) were also synthesized and compared. The analysis results of X-ray diffraction, scanning electron microscopy, and X-ray photoelectron spectroscopy confirmed the formation of FeS_2/Fe_3O_4 composite. The magnetic characterization revealed that the saturation magnetization value for FeS_2/Fe_3O_4 was 50.89 emu g^{-1}, which is helpful for the separation. The effects of the initial pH values, adsorbent dosage, contact time and reaction temperatures on the Cr(VI) removal by various materials were studied and contrasted in detail through experiments. It is found that the composite FeS_2/Fe_3O_4 had high removal capacity for Cr(VI) at high pH. 86.1% of Cr(VI) removal efficiency was obtained when the pH value is at 12.0, the contact time is 3 h and the temperature is controlled at 35°C. FeS_2 component was inferred as the major contribution of the composite to the Cr(VI) removal. FeS_2/Fe_3O_4 displayed a promoted Cr(VI) removal efficiency with the increasing temperature, and its absorption process is proved spontaneous.

Keywords: Adsorption; FeS_2/Fe_3O_4; Pyrite; Fe_3O_4; Cr(VI) removal

1. Introduction

Chromium is one of the most common heavy metal pollutants in wastewater, industrial waste and polluted soil. It usually exists in the form of the hexavalent chromium (Cr(VI) or trivalent chromium (Cr(III). The allowable concentration of total chromium in drinking water was 50 μg L^{-1} by World Health Organization [1,2]. However, the concentration of chromium(VI) in polluted wastewater always far exceeds the safety level [3]. Compared with chromium(III), the toxicity of chromium(VI) is nearly one hundred times higher than that of chromium(III), which due to the formation of insoluble species for Cr(III) such as $Cr(OH)_3$ or $Cr_xFe_{1-x}(OH)_3$ [4,5]. Chromium(VI) is soluble in a wide range of pH environments and can diffuse rapidly in liquid environments. Therefore, it is pressing to develop an effective method to remove Cr(VI) in water.

Reduction and/or adsorption Cr(VI) from the aqueous solution is generally considered as an environmentally friendly and economic technology [6–9]. Among the various adsorbents, Fe_3O_4 has been paid special attention to water purification, because of its simple magnetic separation and mild reaction conditions [10,11]. The structured Fe(II) in Fe_3O_4 has generally been supposed to reduce Cr(VI) to Cr(III), and form a complex chelate on the surface of magnetic particles. Ren et. al. [12] had prepared Fe_3O_4@C using a one-step solvothermal method to remove Cr(VI), and the maximum adsorption capacity was 33.35 mg g^{-1} according to the calculated result, facile magnetic separability and good recyclability also had been proved. Feng et al. [13] synthesized Fe_3O_4

* Corresponding author.

nanoparticles and studied the effects of various conditions for the removal of Cr(VI) in aqueous solution. The maximum adsorption capacity was 56.625 mg g^{-1} at 35°C and the pH value was controlled at 2.0. From the previous reports, the reduction ability of Fe_3O_4 is weak and hard to apply. Its adsorption capacity also presents rather low. Therefore, to remove Cr(VI) successfully using magnetic particles, functionalization and modification of Fe_3O_4 is a practicable tactic.

Natural sulfides are always plentiful and can be used as reductants. Amorphous iron sulfides FeS_2 and FeS have been evaluated for the remediation performance toward hexavalent chromium (Cr(VI)) [14–17]. Theoretically, Cr(VI) reduction reactions occurred on the surface of FeS_x and formed the product. The polysulfide is presumed to be a better electron donor and more effective to remove Cr(VI) from solution. However, the technology may cause secondary pollution, since the reaction product with either sulfide can hardly be collected and treated. $Cr_xFe_{1-x}(OH)_3$ will be oxidized by oxygen and dissolved again in the solution for a long-term treatment trial. Hence, it is necessary to make a functional modification of iron sulfide to satisfy the recyclable needs.

In this work, using a one-pot hydrothermal method, novel magnetic adsorbent FeS_2/Fe_3O_4 was synthesized for the removal of Cr(VI) from aqueous solution. In order to compare the adsorption efficiency, Fe_3O_4 and FeS_2 were also prepared as the adsorbents. The X-ray diffraction, morphology, X-ray photoelectron spectroscopy, and magnetic characterizations were employed to reveal the structure and physical difference among the various materials. The influences of pH value, time and temperature on the adsorption efficiency of Cr(VI) removal were also investigated in detail.

2. Experimental

2.1. Materials and methods

All chemicals in this study were of analytical reagent grade and applied as-receive without further pretreatment. Hexa-hydrate ferric chloride ($FeCl_3·6H_2O$) and ferric nitrate ($Fe(NO_3)_3·9H_2O$) were used as the iron resources of Fe_3O_4 and FeS_2, respectively. Ethylene glycol ($(CH_2OH)_2$), sodium acetate ($C_2H_3NaO_2$), potassium dichromate ($K_2Cr_2O_7$), thiourea (CH_4N_2S), sulfuric acid (H_2SO_4), sodium hydroxide (NaOH), and anhydrous ethyl alcohol (C_2H_5OH) were the analytical reagents purchased from Tianjin Damao Chemical Reagent Co., (Tianjin, China). Double distilled water (18.2 mΩ cm) was used throughout the experiments.

X-ray diffraction (XRD) measurement was performed to confirm the synthesized materials. It was conducted in the 2θ range from 5° and 90° using Cu-Kα radiation with a step size of 0.05° (40 kV, 20 mA; λ = 0.15405 nm). A scanning electron microscopy (SEM) (Zeiss Ultra Plus, Germany) was carried out to study the surface morphologies of samples. The X-ray photoelectron spectroscopy (XPS) spectra of various materials were obtained using ESCALAB 250Xi (Thermo Fisher Scientific Inc., USA) equipped with an Al-Kα monochromated X-ray source (hν = 1,486.6 eV). The Fe 2p peaks were analyzed through XPS Peak. Magnetic measurements were carried out using a vibrating sample magnetometer (Digital Measurement System JDM-13) with a maximum magnetic field of 10,000 O_e at room temperature.

2.2. Preparation of Fe_3O_4 material

The preparation of magnetic nanoparticles was according to the procedures reported in previous researches [3]. In a typical synthesis, 1.35 g $FeCl_3·6H_2O$ was mixed with 40 mL ethylene glycol by stirring under N_2 atmosphere for a period of time. After $FeCl_3$ was completely dissolved, 3.6 g sodium acetate anhydrous was added and stirred continuously to get a transparent solution. Then the mixture was transferred into a 50 mL Teflon lined stainless steel autoclave. The autoclave was heated and maintained at 200°C for 12 h. After the reaction was completed. The black products were cooled naturally, collected by magnetic separation and washed with hot water and ethanol respectively for several times. Finally, the samples were dried in a vacuum oven at 60°C for 12 h, stand by to application.

2.3. Synthesis of FeS_2 and FeS_2/Fe_3O_4 particles

Both FeS_2 and FeS_2/Fe_3O_4 materials were synthesized by using a solvothermal method in our previous report [18]. In brief, the synthesis process was conducted in a 100 mL steel autoclave, which equipped with a temperature controller. The stirring speed for the whole experiment was controlled at 200 rpm. Firstly, 2.0 g $Fe(NO_3)_3·9H_2O$ was dissolved in 40 mL of solvent ethylene glycol, then 1.5 g NH_2CSNH_2 was added and mixed. After being dissolved, the reactants were then put into the reactor. The autoclave was sealed and heated subsequently. The temperature was kept constant at 200°C for 48 h. When the reaction was finished, the autoclave was cooled naturally, the black powder was obtained via vacuum filter and washed three times with distilled water and ethanol, respectively. Finally, the synthetic product was dried under argon flow at 60°C for 8 h to get the FeS_2 powder for future use.

The preparation of FeS_2/Fe_3O_4 materials is similar to FeS_2 synthesis procedures. The appropriate amount of as-prepared Fe_3O_4 was dispersed in the solvent ethylene glycol, then $Fe(NO_3)_3·9H_2O$ and NH_2CSNH_2 were added and dissolved in turn. The following operation was the same as described in the pyrite preparation. The mole ratio of FeS_2 to Fe_3O_4 was controlled at 1:1.

2.4. Adsorption experiments

The synthetic Fe_3O_4, FeS_2/Fe_3O_4, and FeS_2 particles were applied to remove Cr(VI). The Cr(VI) solution (100 mg L^{-1}) was prepared by dissolving 0.2827 g of stock $K_2Cr_2O_7$ with 1,000 mL deionized water and kept away from sunlight. The reaction volume of Cr(VI) solution was 50 mL for all the experiments. The 1, 5-diphenylcarbazide (DPC) spectrophotometric method, which is an international standard for the determination of chromium(VI) in waters, was applied to settle the Cr(VI) concentration at 540 nm during the whole tests. The desired adsorption conditions, such as initial pH value, adsorbent dosage, contact time and temperature were researched in detail. The initial pH values were ranged from 2.0 to 12.0, and the adjustment reagent was 0.5 M H_2SO_4 or 0.5 M NaOH. The adsorbent dosages were performed at 0.2, 0.3, 0.4, 0.6, and 0.8 g L^{-1}, respectively. The contact times of various materials were conducted at 1, 2, 3, 4, 5, and 6 h,

respectively. The temperature was changed from 25°C to 45°C. After adsorption finished, Fe_3O_4 and FeS_2/Fe_3O_4 materials were removed from the solution by magnetic separation, the pyrite was separated centrifugally.

3. Results and discussion

3.1. Characterization of the synthetic materials

XRD patterns of the different powders are shown in Fig. 1. The Bragg diffraction peaks of FeS_2 and Fe_3O_4 can be perfectly confirmed as one single-phase (JCPDS card No. 42–1340 and 88–0315). No peaks of other iron sulfides and oxides, such as marcasite (FeS_2), troilite (FeS) and hematite (Fe_2O_3), are observed in XRD patterns. The two samples were both cubic structures, and the space groups were indexed to Pa3 [205] and Fd-3m [227], respectively. From Fig. 1, it is obviously noted that the observable reflections of FeS_2/Fe_3O_4 contained has strong and sharp diffraction peaks for both FeS_2 and Fe_3O_4. For example, the peaks at 2θ values of 28.51°, 33.08°, 37.10°, 40.78°, and 47.41° were indexed to the crystallographic planes (111), (200), (210), (211) and (220) of FeS_2, respectively. While those peaks located at 30.15°, 35.52°, 43.17°, 57.09°, and 62.70° were (220), (311), (400), (511), and (440) planes of Fe_3O_4. Thus, it is inferred the novel FeS_2/Fe_3O_4 has been successfully synthesized. The hydrothermal synthesis was proved to be a reliable method to prepare pure iron sulfide or oxide.

The morphology and the change of detailed microstructure for the three materials are illustrated by SEM images, as shown in Fig. 2. From Fig. 2a, Fe_3O_4 particles exhibit the morphology of regular octahedra with a particle size range of about 2–8 μm. SEM image of FeS_2 in Fig. 2b indicated the synthetic pyrite material was composed of particle agglomeration, the small first particle was all irregular sphere with 2–6 μm in diameters. It is interesting to learn that the composite FeS_2/Fe_3O_4 presents the mixed characteristics of the former two materials. The structures of particle agglomeration and regular octahedra are both maintained in the material. However, the particle agglomeration of pyrite decreased and the size became smaller by adding Fe_3O_4 suspension.

XPS spectra are shown in Fig. 3 were used to further analyze the surface compositions of the three materials. Two peaks can be detected in the XPS spectrum of Fe 2p for Fe_3O_4 (Fig. 3a). The peak at 710.0 eV is ascribed to Fe(II), and the shoulder peak found at 724.1 eV can be attributed to Fe(III), which suggested the co-existence of Fe(III) and Fe(II) in the synthetic Fe_3O_4. Three major peaks can be observed in the XPS spectrum of Fe 2p for FeS_2 (Fig. 3b). The peaks appeared at 706.7 eV and 711.3 eV are related to Fe 2p3/2, and the peak at 720.3 eV matches well with Fe 2p1/2, which is confirmed as the characteristic of FeS_2. It is

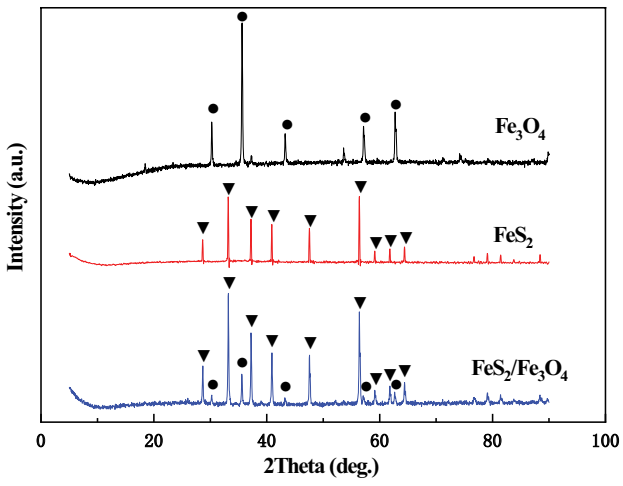

Fig. 1. XRD patterns for (a) Fe_3O_4, (b) FeS_2, and (c) FeS_2/Fe_3O_4.

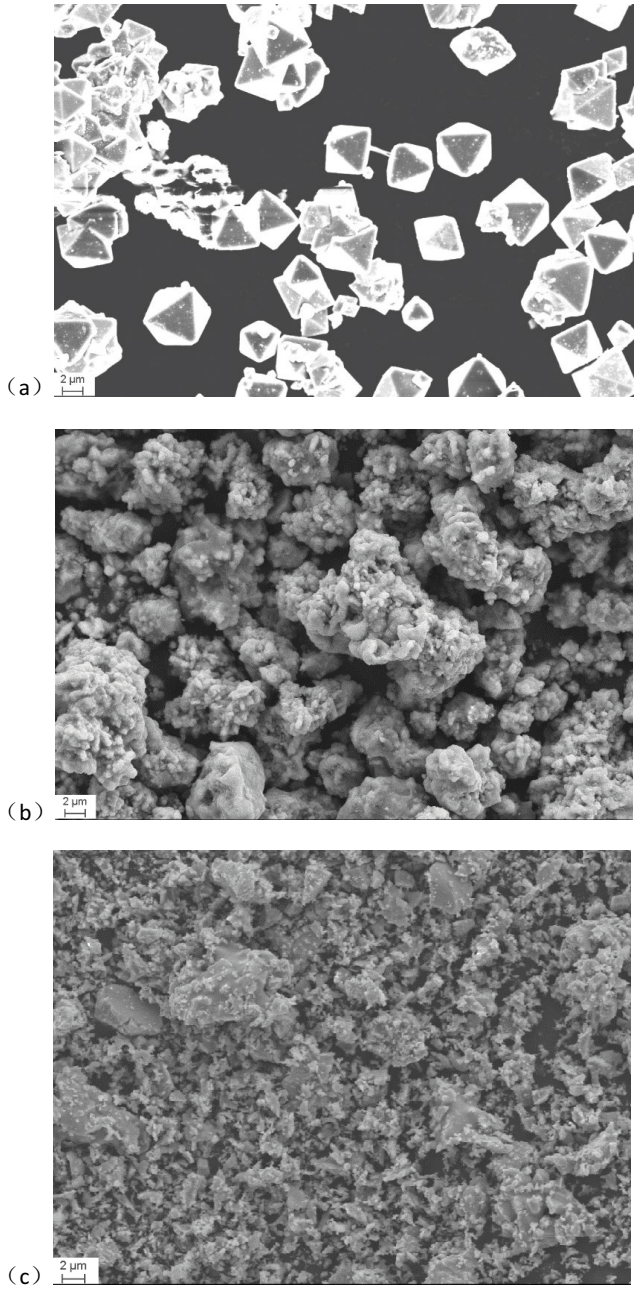

Fig. 2. SEM images of (a) Fe_3O_4, (b) FeS_2, and (c) FeS_2/Fe_3O_4.

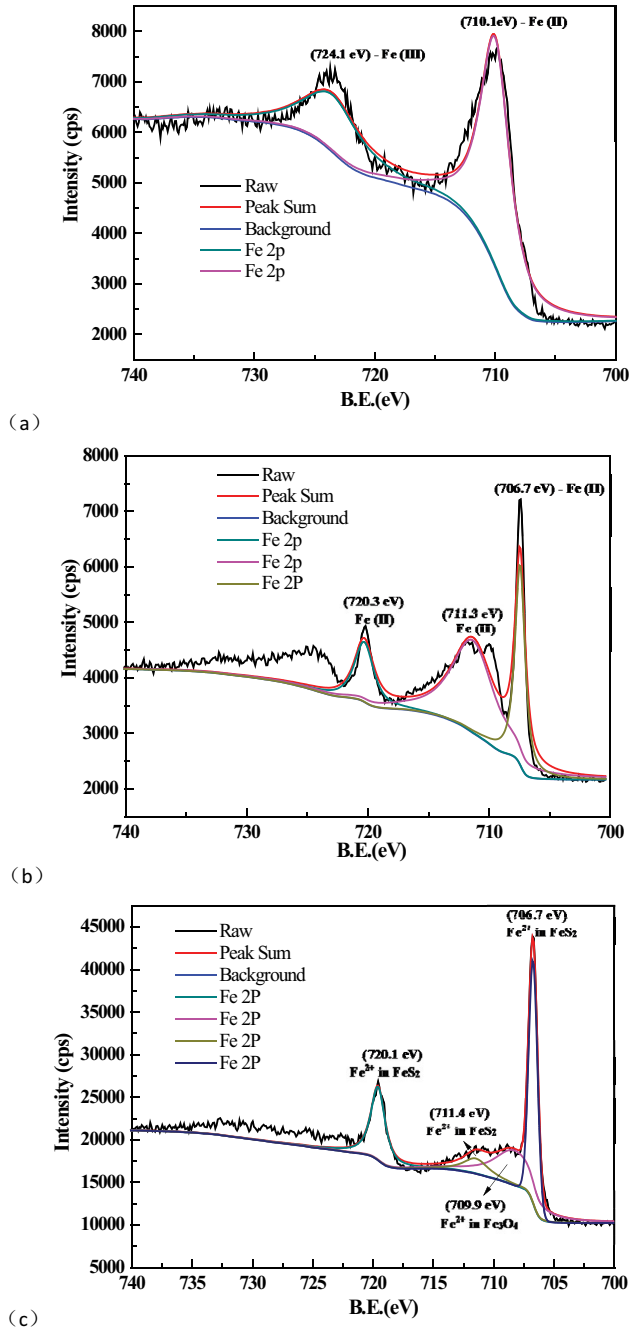

Fig. 3. Fe XPS Spectra of (a) Fe_3O_4, (b) FeS_2, and (c) FeS_2/Fe_3O_4.

easily observed and calculated from Fig. 3c that there are four peaks (720.1, 711.4, 709.9, and 706.7 eV) of Fe 2p for FeS_2/Fe_3O_4. It means FeS_2/Fe_3O_4 composite contains both the characteristic of FeS_2 and Fe_3O_4. Nevertheless, the XPS spectrum of a composite is more similar than that of FeS_2, which may be due to that Fe_3O_4 has been applied as the basic core material, and the pyrite was formed on its surface. This makes the surface concentration of the two type iron different for FeS_2/Fe_3O_4.

Fig. 4 shows the magnetic property of different samples. The saturation magnetization (M), showing in the hysteresis

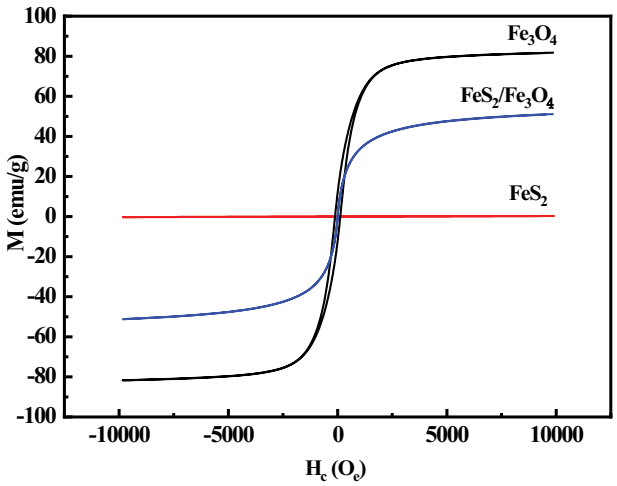

Fig. 4. Magnetization–hysteresis (M–H) loops of Fe_3O_4, FeS_2 and FeS_2/Fe_3O_4 measured at room temperature.

loop of magnetic material, demonstrates the complete magnetizability of test materials. It is apparently found the FeS_2 has no magnetic property. The saturation magnetization value for FeS_2/Fe_3O_4 was 50.89 emu g^{-1}. The decrease is about 37% comparing to the saturation magnetization of Fe_3O_4. This is caused by the less concentration of magnetite the in the composite. Even so, the separation of FeS_2/Fe_3O_4 from the solution can be finished successfully and quickly.

3.2. Removal of Cr(VI) with synthetic materials

The as-prepared materials were used for the removal of aqueous Cr(VI) at various pH values range from 2.0 to 12.0. Fig. 5 shows experimental data for the influence of pH value on Cr(VI) adsorption. It was observed that the Cr(VI) removal efficiency with FeS_2 fell down quickly from the initial 96.9% with the increasing pH value. The lowest Cr(VI) removal efficiency reached to 34.1% for pyrite material when the pH was controlled at 12.0. In the previous researches, different reaction mechanism had been proposed to understand the Cr(VI) removal process. The consensus view is that Cr(VI) is reduced to Cr(III) by pyrite, Fe(II) and S_2^{2-} are oxidized to Fe(III) and SO_4^{2-}, respectively. Besides, some intermediate products such as elemental sulfur can be formed during the reaction:

$$3FeS_2 + 3HCrO_4^- + 21H^+ = 3Fe^{3+} + 6S^0 + 3Cr^{3+} + 12H_2O \quad (1)$$

$$3FeS_2 + 15HCrO_4^- + 57H^+ = 3Fe^{3+} + 6SO_4^{2-} + 15Cr^{3+} + 36H_2O \quad (2)$$

According to Eqs. (1) and (2), acidic conditions are considered to favor the Cr(VI) reduction by pyrite. The higher pH could induce the Fe- or Cr-hydroxides precipitate on FeS_2 material and lead to surface passivation. Furthermore, since the product Fe(III) is a strong oxidizing agent, it would be expected to speed up the pyrite dissolution in lower pH values. The solution pH also can influence the existence of Cr species. CrO_4^- is the major Cr(VI) state under the alkaline

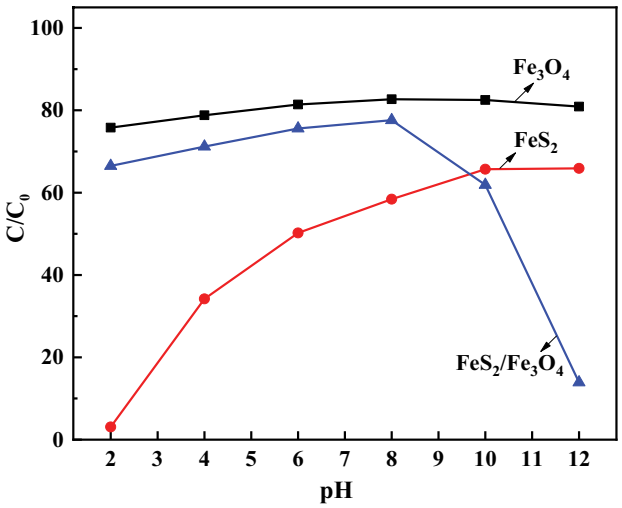

Fig. 5. Effect of pH value on Cr(VI) removal with Fe_3O_4, FeS_2/Fe_3O_4 and FeS_2 (Contact time = 3 h, initial Cr(VI) concentration = 100 mg L^{-1}, T = 35°C).

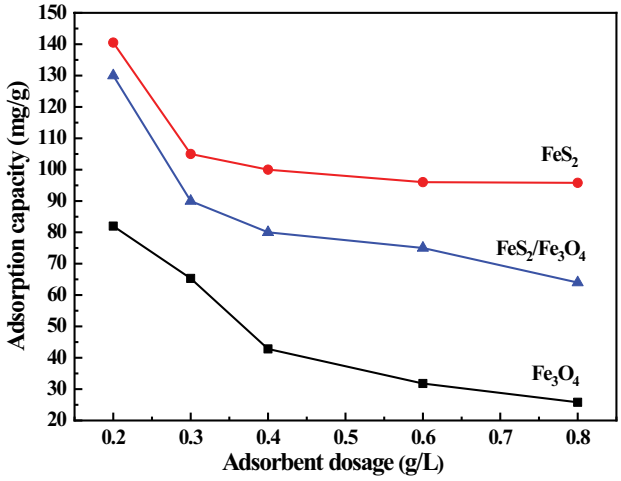

Fig. 6. Effect of adsorbent dosage on Cr(VI) removal with Fe_3O_4, FeS_2/Fe_3O_4 and FeS_2 (Contact time = 3 h, initial Cr(VI) concentration = 100 mg L^{-1}, T = 35°C, pH for Fe_3O_4, FeS_2/Fe_3O_4 and FeS_2 were 2, 12, and 2, respectively).

condition, and the dominant reduction product is Cr(III)-OH [19]. It was evident that the removal ratio of Cr(VI) was lowly pH-dependent for Fe_3O_4. This could be attributed to weaker reductively comparing to the pyrite. Another reason could be that the surfaces of regular octahedral magnetite particles are the smoother and less micro-pore structure, as shown in Fig. 2. The removal efficiency of Cr(VI) from aqueous solution ranged from only 17.3% to 24.2% for the whole pH values, much lower than that applying FeS_2. It was worth noting that the solution pH has been observed as one of the important parameters affecting the Cr(VI) removal. It is interesting to find that Cr(VI) removal efficiency dramatically enhances from 22.4% to 86.1% when the pH value increased from 8.0 to 12.0. The reason could be explained as follows, the presence of Fe_3O_4 decreased the formation of Fe–Cr hydroxides at higher pH values, and the formed discontinuous intermediate products on the composite surface, such as elemental sulfur, Fe–S, and Fe–OH, may owe strong adsorption capacity of CrO_4^{2-} under alkaline conditions.

The effects of adsorbent dosage on Cr(VI) removal with Fe_3O_4, FeS_2/Fe_3O_4, and FeS_2 were displayed, and the results are shown in Fig. 6. The adsorption capacity of Cr(VI) for the three synthetic materials declined rapidly with the augment in adsorbent dosage from 0.2 to 0.4 g L^{-1}. The highest adsorption capacities of Cr(VI) for Fe_3O_4, FeS_2/Fe_3O_4 and FeS_2 were 82.0, 130, and 141 mg g^{-1}, respectively. With a further increase in the adsorbent dosage from 0.4 to 0.8 g L^{-1}, the change of Cr(VI) removal capacity became slow. FeS_2 and Fe_3O_4 gained the max and the min Cr(VI) removal capacity respectively for the same adsorbent dosage. This is in agreement with the previous analysis.

To get adsorption isotherms for the synthetic materials, Langmuir isotherm and Freundlich isotherm models were used to fitting the data. The adsorption properties of the adsorbent at 298 K, an adsorbent concentration of 0.6 g L^{-1}, initial Cr(VI) concentration was ranged from 10 to 200 mg L^{-1}, were analyzed by using the Langmuir model and Freundlich model. The Langmuir isotherm model is applicable for monolayer adsorption on a surface containing a finite number of binding sites. The linear form of the Langmuir equation is written as Eq. (3):

$$\frac{C_e}{q_e} = \frac{C_e}{q_m} + \frac{1}{\left(q_m K_L\right)} \tag{3}$$

where q_m is the maximum capacity of adsorbent (mg g^{-1}) and K_L is the Langmuir adsorption constant (L mg^{-1}). The Freundlich isotherm model, which is based on the assumption that the adsorption occurs on a heterogeneous adsorbent surface, can be represented as Eq. (4):

$$\ln q_e = \ln K_F + \frac{1}{n}\ln C_e \tag{4}$$

where K_F and n are the Freundlich constants related to the maximum adsorption capacity (mg g^{-1}) and the heterogeneity factor (m g^{-1}), respectively. They can be obtained from the slope and intercept of the linear plot of $\ln q_e$ vs. $\ln C_e$.

The two models were used to fit and analyze the tested data (Fig. 7 and Table 1). The results show that the Langmuir model can better explain the adsorption onto FeS_2 and Fe_3O_4, while the Freundlich model is more suitable to the FeS_2/Fe_3O_4.

The effect of contact time on the removal of 100 mg L^{-1} Cr(VI) with the as-prepared materials was conducted at their optimal pH value and the temperature was 35°C. As shown in Fig. 8, obviously, the adsorption capacity of all three materials raised quickly with the prolonging contact time from 0 to 3 h. When the reaction time was more than 4 h, the adsorptive equilibrium of anoxic Cr(VI) was mainly achieved. The equilibrium adsorption capacities of Cr(VI) for Fe_3O_4, FeS_2/Fe_3O_4 and FeS_2 were 25.5%, 89.5%, and 98.7%, respectively.

To study the mechanism of the adsorption process and determine the factors controlling the adsorption diffusion,

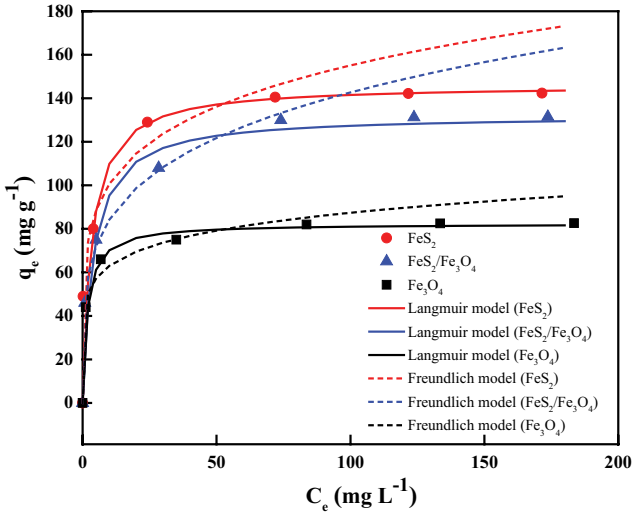

Fig. 7. Adsorption isotherm fitting diagram.

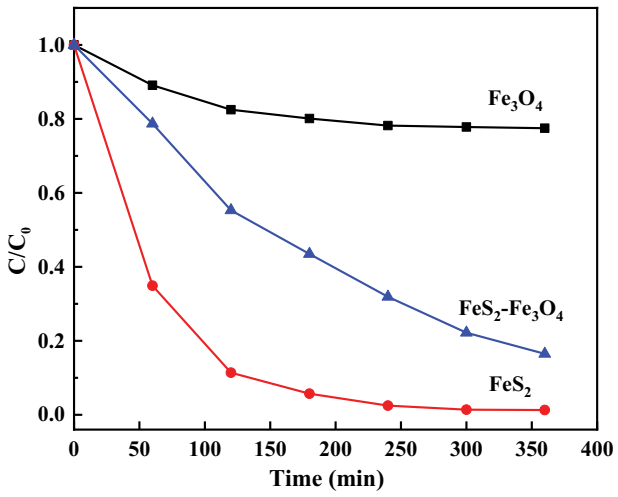

Fig. 8. Effect of contact time on Cr(VI) removal with Fe_3O_4, FeS_2/Fe_3O_4 and FeS_2 (Contact time = 3 h, initial Cr(VI) concentration = 100 mg L^{-1}, T = 35°C, pH for Fe_3O_4, FeS_2/Fe_3O_4 and FeS_2 were 2, 12, and 2 respectively).

the data for Cr(VI) adsorption with different initial concentrations of the pollutant were analyzed by using the intraparticle diffusion model. The intraparticle diffusion model Eq. (5) is as follows:

$$q_t = k_1 t^{0.5} + C \tag{5}$$

where q_t (mg g^{-1}) is the adsorption capacity at the time, t; k_1 (mg g^{-1} min$^{0.5}$) is the intraparticle diffusion rate constant; and C is the model constant. The model Eqs. (6) and (7) of Boyd diffusion model are as follows:

$$F = \frac{q_t}{q_e} \tag{6}$$

$$\ln(1-F) = -k_2 t \tag{7}$$

where F is the fractional attainment of equilibrium at different times, k_2 is a mathematical function of F. By fitting the data with the intraparticle diffusion model (Fig. 9 and Table 2). It was found that the orders of adsorption rate are as follows: $k_{1(FeS_2)} > k_{1(FeS_2/Fe_3O_4)} > k_{1(Fe_3O_4)}$, $k_{2(FeS_2)} > k_{2(FeS_2/Fe_3O_4)} > k_{2(Fe3O4)}$. It is also can be noted that the Boyd diffusion model is more consistent for the adsorption processes onto FeS_2 and FeS_2/Fe_3O_4, and the internal diffusion is found as the main diffusion process for Fe_3O_4.

Adsorption temperature is another key influence factor for the removal of Cr(VI) from aqueous solution. Thus the effect of temperature on the Cr(VI) absorption was displayed with the temperature ranged from 25°C to 45°C, other experimental conditions such as the contact time and the initial Cr(VI) concentration were kept the same. The test results were shown in Fig. 10, it is observed that the adsorption capacity of Fe_3O_4 for Cr(VI) ions decreased slightly, no more than 8%, with increasing temperature. By contrast, the adsorption capacities for both FeS_2/Fe_3O_4 and FeS_2 enhanced about 20% when raising the temperature by 20°C. It is inferred that higher temperature has the advantage of the promotion adsorption process of Cr(VI) onto FeS_2/Fe_3O_4 and FeS_2, and the reaction was controlled by an endothermic nature.

To further understand the adsorption mechanism, the thermodynamic equilibrium constants K_c of the adsorption process were calculated (Fig. 11 and Table 3). The change in Gibbs free energies (ΔG, kJ mol^{-1}), the adsorption heat (ΔH, kJ mol^{-1}) and the adsorption entropy change (ΔS, kJ (K^{-1} mol^{-1})) was calculated accordingly. Eqs. (8)–(10) are as follows:

$$K_c = \frac{q_c}{q_e} \tag{8}$$

Table 1
Langmuir and Freundlich isotherm constants for the adsorption of Cr(VI) onto the synthetic materials

Materials	Langmuir			Freundlich		
	q_m (mg g^{-1})	K_L (L mg^{-1})	R^2	n	K_F (L g^{-1})	R^2
Fe_3O_4	82.37	0.5756	0.9354	7.05	45.47	0.9337
FeS_2	146.2	0.3023	0.9998	5.33	65.38	0.9836
FeS_2/Fe_3O_4	132.2	0.2581	0.9766	4.36	49.74	0.9949

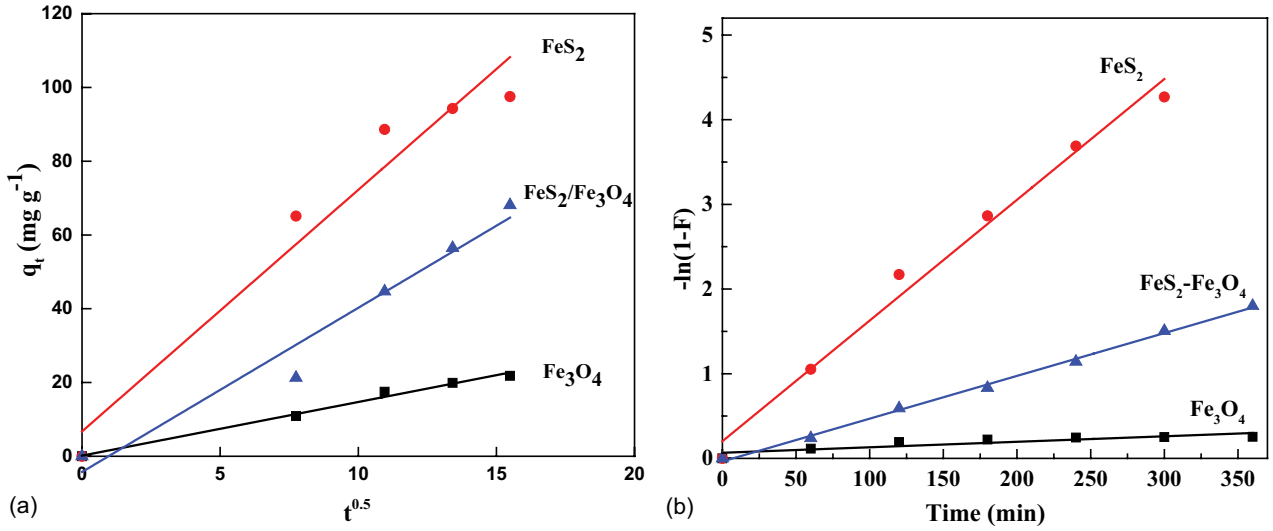

Fig. 9. (a) Intraparticle diffusion model and (b) Boyd diffusion model diagrams.

Table 2
Intraparticle diffusion and Boyd diffusion kinetic parameters for the adsorption of Cr(VI) onto the synthetic materials

Materials	Intraparticle diffusion model		Boyd diffusion model	
	k_1	R^2	k_2 (×10^4)	R^2
Fe_3O_4	1.455	0.9867	6.48	0.7523
FeS_2	6.549	0.9354	143	0.9841
FeS_2/Fe_3O_4	4.451	0.9512	50.5	0.9970

$$\Delta G = -RT\ln K_c \quad (9)$$

$$\log K_c = \frac{\Delta S}{2.303R} - \frac{\Delta H}{2.303RT} \quad (10)$$

where K_c is the equilibrium constant; q_c (mg L^{-1}) is the concentration of metal ions in aqueous solution at equilibrium; q_e (mg g^{-1}) is the equilibrium adsorption capacity of adsorbent; R (8.314 J (mol^{-1} K^{-1})) is the universal gas constant; T (K) is the temperature.

Table 3 shows the thermodynamic parameters. The free energy change (ΔG) for Fe_3O_4 is positive, while those for the other two materials were negative. It is also noted that the absolute values all increase with increasing temperature. Thus the adsorption processes applying FeS_2 and FeS_2/Fe_3O_4 are proved spontaneous and the high the temperature can

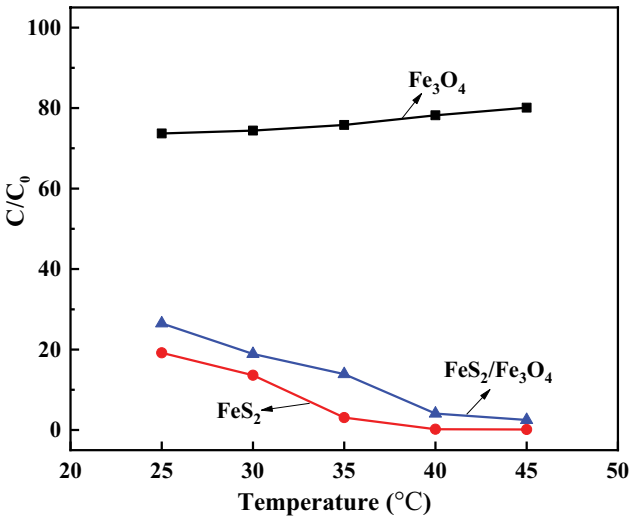

Fig. 10. Effect of temperature on Cr(VI) removal with Fe_3O_4, FeS_2/Fe_3O_4, and FeS_2 (Contact time = 3 h, initial Cr(VI) concentration = 100 mg L^{-1}, pH for Fe_3O_4, FeS_2/Fe_3O_4 and FeS_2 were 2, 12, and 2, respectively).

Table 3
Thermodynamic parameters for the adsorption of various samples

Materials	ΔH (kJ mol^{-1})	ΔS (KJ (K^{-1} mol^{-1}))	ΔG (kJ mol^{-1})				
			T = 298 K	T = 303 K	T = 308 K	T = 313 K	T = 318 K
Fe_3O_4	–14.45	–0.057	2.55	2.69	2.92	3.32	3.68
FeS_2	223.8	0.759	–3.56	–4.66	–8.81	–16.2	–17.2
FeS_2/Fe_3O_4	107.9	0.368	–2.53	–3.67	–4.67	–8.20	–9.69

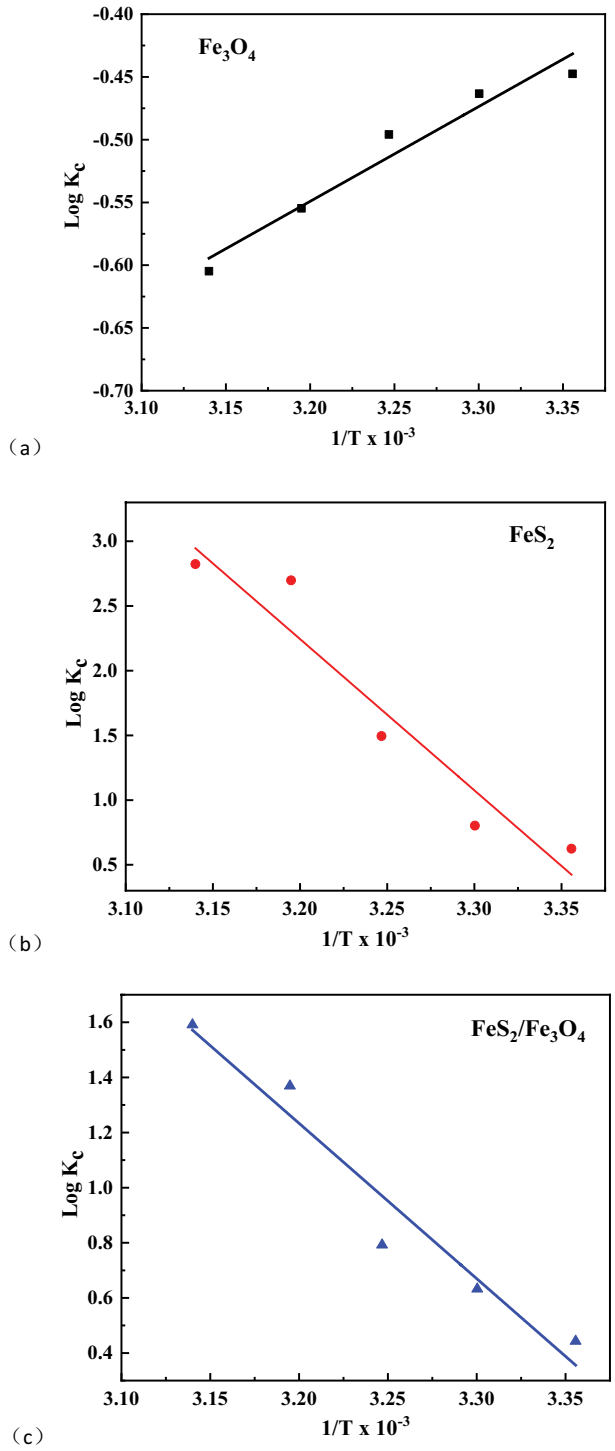

Fig. 11. LogK_c–1/T of various samples: (a) Fe_3O_4, (b) FeS_2, and (c) FeS_2/Fe_3O_4.

enhance the adsorption reaction. From the calculated results, the addition of Fe_3O_4 will weaken the adsorption speed of Cr(VI) due to that its adsorption process is nonspontaneous and exothermic. The positive entropy change ΔS for the three materials implies that, after reaching adsorption equilibrium, the degree of disorder for the liquid increased, which may be ascribed to the increase of species number at the solid/liquid interface.

4. Conclusion

In summary, Fe_3O_4, FeS_2, and FeS_2/Fe_3O_4 have been successfully synthesized for removal of Cr(VI) from water solution. The obtained FeS_2/Fe_3O_4 includes composite morphological characteristics for both Fe_3O_4 and FeS_2. It also exhibits strong magnetism as fabricated and easily separated from the solution after adsorption. The adsorption capacities for Fe_3O_4, FeS_2, and FeS_2/Fe_3O_4 were 82.0, 141, and 130 mg g^{-1}, respectively, showing that FeS_2/Fe_3O_4 has both high adsorption capacities and convenient magnetic separation. The optimal conditions for FeS_2/Fe_3O_4 to remove Cr(VI) were that the contact time is 3 h and the pH value is 12. The kinetics of adsorption indicates that the adsorption process of Cr(VI) using either FeS_2 or FeS_2/Fe_3O_4 is spontaneous and the high the temperature can enhance the adsorption reaction. The study will provide a basis for designing composite of sulfide and magnetic Fe_3O_4 with controlled morphology and porous structures for practical environmental applications.

Acknowledgments

This work was supported by the National Key R&D Program of China (2018YFC1902003), the Fundamental Research Funds for the Central Universities (N172504022), and the National College Students Innovation Project of China (180077).

References

[1] X. Huang, Y. Liu, S. Liu, X. Tan, Y. Ding, G. Zeng, Y. Zhou, S. Wang, M. Zhang, B. Zheng, Effective removal of Cr(VI) using β-cyclodextrin-chitosan modified biochars with adsorption/reduction bifunctional roles, RSC Adv., 6 (2015) 94–104.
[2] H.H. Lyu, J.C. Tang, Y. Huang, L.S. Gai, E.Y. Zeng, K. Liber, Y.Y. Gong, Removal of hexavalent chromium from aqueous solutions by a novel biochar supported nanoscale iron sulfide composite, Chem. Eng. J., 322 (2017) 516–524.
[3] Z.B. Zhang, H.F. Duan, S.H. Li, Y.J. Lin, Assembly of magnetic nanospheres into one-dimensional nanostructured carbon hybrid materials, Langmuir, 26 (2010) 6676–6680.
[4] X. Tian, K. Patel, J.R. Ridpath, J.A. Swenberg, J. Nakamura, Genotoxicity of trace level of hexavalent chromium existing in city water, Cancer Res., 74 (2014) 5363–5364.
[5] S.A. Katz, H. Salem, The toxicology of chromium with respect to its chemical speciation: a review, J. Appl. Toxicol., 13 (1993) 217–224.
[6] H.S. Chang, J.H. Singer, J.C. Seaman, In-situ chromium (VI) reduction using iron (II) solutions: modeling dynamic geochemical gradients, Vadose Zone J., 11 (2012) 1043–1053.
[7] M. Pettine, D. Tonnina, F.J. Millero, Chromium (VI) reduction by sulfur (IV) in aqueous solutions, Mar. Chem., 99 (2006) 31–41.
[8] C. Kantar, C. Ari, S. Keskin, Z.G. Dogaroglu, A. Karadeniz, A. Alten, Cr (VI) removal from aqueous systems using pyrite as the reducing agent: batch, spectroscopic and column experiments, J. Contam. Hydrol., 174 (2015) 28–38.
[9] Q. Liu, M.J. Xu, F. Li, T. Wu, Y.J. Li, Rapid and effective removal of Cr(VI) from aqueous solutions using the $FeCl_3$/$NaBH_4$ system, Chem. Eng. J., 296 (2016) 340–348.
[10] D.L. Zhao, X. Gao, C.N. Wu, R. Xie, S.J. Feng, C.L. Chen, Facile preparation of amino-functionalized graphene oxide decorated

with Fe_3O_4 nanoparticles for the adsorption of Cr(VI), Appl. Surf. Sci., 384 (2016) 1–9.
[11] X. Xin, Q. Wei, J. Yang, L. Yan, R. Feng, G. Chen, B. Du, H. Li, Highly efficient removal of heavy metal ions by amine-functionalized mesoporous Fe_3O_4 nanoparticles, Chem. Eng. J., 184 (2012) 132–140.
[12] L. Ren, H.X. Lin, F.C. Meng, F. Zhang, One-step solvothermal synthesis of Fe_3O_4@carbon composites and their application in removing of Cr(VI) and Congo red, Ceram. Int., 45 (2019) 9646–9652.
[13] Y.B. Feng, Y. Du, Z.T. Chen, M.X. Du, K. Yang, X.J. Lv, Z.F. Li, Synthesis of Fe_3O_4 nanoparticles with tunable sizes for the removal of Cr(VI) from aqueous solution, J. Coat. Technol. Res., 15 (2018) 1145–1155.
[14] Y.Y. Li, J.L. Liang, Z.H. Yang, H. Wang, Y.S. Liu, Reduction and immobilization of hexavalent chromium in chromite ore processing residue using amorphous FeS_2, Sci. Total Environ., 658 (2019) 315–323.
[15] Y.Y. Li, J.L. Liang, X. He, L. Zhang, Y.S. Liu, Kinetics and mechanisms of amorphous FeS2 induced Cr(VI) reduction, J. Hazard. Mater., 320 (2016) 216–225.
[16] E.A. Kaprara, A.I. Zouboulis, K.T. Simeonidis, M.G. Mitrakas, Potential application of inorganic sulfur reductants for Cr(VI) removal at sub-ppb level, Desal. Water Treat., 54 (2015) 2067–2074.
[17] Y.Y. Li, A.B. Cundy, J.X. Feng, H. Fu, X.J. Wang, Y.S. Liu, Remediation of hexavalent chromium contamination in chromite ore processing residue by sodium dithionite and sodium phosphate addition and its mechanism, J. Environ. Manage., 192 (2017) 100–106.
[18] G.B. Chen, Z.F. Zhu, Y. Qin, Synthesis of pure micro- and nanopyrite and their application for As(III) removal from aqueous solution, Adv. Mater. Sci. Eng., 2016 (2016) 6290420.
[19] W. Liu, L.D. Jin, J. Xu, J. Liu, Y.Y. Li, P.P. Zhou, C.C. Wang, R.A. Dahlgren, X.D. Wang, Insight into pH-dependent Cr(VI) removal with magnetic Fe_3S_4, Chem. Eng. J., 359 (2019) 564–571.